Electronic Supplementary Information

Zn^{2+} Conductive-Hydrophilic Lanthanum Phosphate Interlayer toward Ultra-Long-Life Zn Anodes and Zinc Ion Capacitors

Yuequn Li,[a] Yanjie Wang,*[a,b] Zhe Fang,[a] Shaopei Jia,[a] Xukai Wu,[a] Zhiheng Wang,[a] Kunyang Geng,[a] Kongyao Chen, *[b] Yunchao Mu,[a] Lin Zhang[b] and Liwei Mi*[b,c]

[a] School of Materials Electronics and Energy Storage, Zhongyuan University of Technology, Zhengzhou 45007, P. R. China

[b] Henan Key Laboratory of Functional Salt Materials, Center for Advanced Materials Research, Zhongyuan University of Technology, Zhengzhou 45007, P. R. China

[c] Yaoshan laboratory, Pingdingshan 467000, P. R. China

*Corresponding author(s): wangyj6527@zut.edu.cn (Yanjie Wang), chenkongyao@zut.edu.cn (Kongyao Chen), mlwzzu@163.com (Liwei Mi)

Experimental Section

Preparation of $LaPO_4$: 20.3 g $(NH_4)_3PO_4$ (AR, 98.0%) was dissolved in 100 mL of H_2O to obtain the $(NH_4)_3PO_4$ solution. 43.31 g of $La(NO_3)_3 \cdot H_2O$ (AR, 98.0%) was dissolved in 100 mL H_2O to obtain $La(NO_3)_3$ solution. Then the $(NH_4)_3PO_4$ solution was added to the $La(NO_3)_3$ solution, and the mixture was heated at 50 ^oC for 30 min. The $LaPO_4$ powder was then obtained by centrifugation and vacuum drying at 70 ^oC for 24 h.

Preparation of LAP-Zn anode: $LaPO_4$ powder and PVDF (9:1 mass ratio) were mixed and ground for 30 min. Later, an appropriate amount of 1-Methyl-2-pyrrolidinone (NMP) was added, and the mixture was ground for another 30 min to obtain a uniform slurry. Subsequently, the uniform slurry was coated on a clean Zn foil (0.1 mm thickness). The LAP-Zn anode was obtained after drying at 70 ^oC for 12 h in a vacuum oven.

Material characterization

A Scanning Electron Microscope (SEM, Merlin compact (Zeiss Merlin, Germany)) equipped with an Energy Dispersive X-ray Spectrometer (EDS) was used to analyze the morphology and elemental distribution of the samples, respectively. The phase and structure of the samples were characterized by X-ray Diffraction (XRD, Rigaku Ultima IV) in the Cu K-α wave range of 10° to 90° with a scan rate of 10° min^{-1}. A Contact Angle Meter (OCA200, Beijing Data Instrument Co., Ltd.) was used to measure the wettability of H_2O or electrolyte on the electrode surface. The Vienna Ab Initio Package (VASP) was used to calculate the adsorption energy between H_2O and $LaPO_4$ or Zn. The *in-situ* observation of Zn deposition process was carried out through a transparent Zn//Zn cell and the Zn^{2+} migration number was calculated by impedance value of symmetric cells before and after a polarization process at a constant potential of 10 mV for 400 s.

Assembly and electrochemical measurement of electrochemical devices

Assembly of CR2032 type LAP-Zn//LAP-Zn symmetric cells: The LAP-Zn//LAP-Zn symmetrical cell was assembled by selecting two LAP-Zn electrode sheets (8 mm) as the working electrode and counter electrode, 2 M $ZnSO_4$ solution as the electrolyte, and glass fiber paper as the separator. The assembly process of the Zn//Zn symmetric cells is similar to that of the LAP-Zn//LAP-Zn symmetrical cells except for choosing pure Zn as the electrode sheets (8 mm).

Assembly of CR2032 type LAP-Zn//LAP-Zn half cells: The assembly process of CR2032 type LAP-Zn//Cu and Zn//Cu half cells is similar to that of the symmetric cells except for a titanium (Ti) electrode (thickness 20 μm, diameter 8 mm) that is used as the working electrode.

Preparation of AC Electrode Sheet: AC (purchased from Xianfeng Nano), acetylene black, and PVDF were mixed in a 7:2:1 mass ratio in NMP, and the resultant slurry was coated on a Ti foil. After drying at 70 °C for 12 h, the AC electrode was obtained, which was then cut into AC electrode sheets of 8 mm diameter. The loading amount of AC is approximately 1-2 mg cm^{-2}.

Assembly of CR2032-type LAP-Zn//AC Zinc Ion Capacitor: The LAP-Zn//AC zinc ion capacitors were assembled by choosing the AC electrode as the cathode, LAP-Zn as the anode, 2 M $ZnSO_4$ solution as the electrolyte, and glass fiber paper as the separator. The assembly process of Zn//AC is similar to that of LAP-Zn//AC, except that Zn is the anode.

Electrochemical Measurement: The long-term cycling stability and rate performance were carried out on a LAND battery test system (CT2001A-type battery tester, Wuhan Blue Sky Electronics Co., LTD.). The Electrochemical Impedance Spectroscopy (EIS), Cyclic Voltammetry (CV), and current-time curves were obtained using a CHI600E electrochemical workstation (Shanghai Chenhua Co. LTD). To study the influence of LAP on HER and Zn corrosion side reactions, linear polarization curves and linear sweep

voltammetry (LSV) curves were obtained using the workstation with Zn or LAP-Zn as the working electrode, platinum as the counter electrode, and Ag/AgCl as the reference electrode. The scanning voltage range of LSV curves is -1.4 to -2 V. The linear polarization curve was tested at a scan rate of 1 mV s^{-1} in the voltage range of -0.2 to -1.2 V (relative to the Ag/AgCl electrode).

The Zn^{2+} transference number (t_{Zn2+}) of Zn symmetrical cell was measured through chronoamperometry (CA) and electrochemical impedance spectroscopy (EIS), and calculated according to the following equation:

$$t_{Zn^{2+}}=\frac{(\Delta V/I_0-R_0)}{(\Delta V/I_{SS}-R_{SS})} \quad \text{(S1)}$$

Δ V is constant potential of 10 mV. I_0 represents the initial response current. I_{ss} is the steady-state response current. R_0 and R_{ss} are the electrode interface impedances before and after polarization, respectively.

Computational method: The spin-polarized DFT were conducted through the Vienna Ab Initio Package (VASP) with the projector augmented wave (PAW) method [1, 2]. The exchange-functional is treated using the generalized gradient approximation (GGA) with Perdew-Burke-Ernzerhof (PBE) functional [3]. The energy cutoff for the plane wave basis expansion was 450 eV. Partial occupancies of the Kohn—Sham orbitals were allowed using the Gaussian smearing method and a width of 0.1 eV. The H_3LaPO_4 cluster was built with exposed (1 0 2) surface. The Brillouin zone was sampled with Monkhorst mesh of $2\times2\times1$ for the optimization for all the structures. The self-consistent calculations apply a convergence energy threshold of 10^{-5} eV, and the force convergency was set to 0.05 eV/Å. Moreover, the adsorption energy (Eads) was expressed as follows,

Eads = Ecomplex - Esurf - EZn

where Ecomplex, Esurf and EZn are the energy of the Zn adsorbed on the H_3LaPO_4 slab or the H_2O, the

energy of H_3LaPO_4 slab or the H_2O, and the energy of Zn respectively.

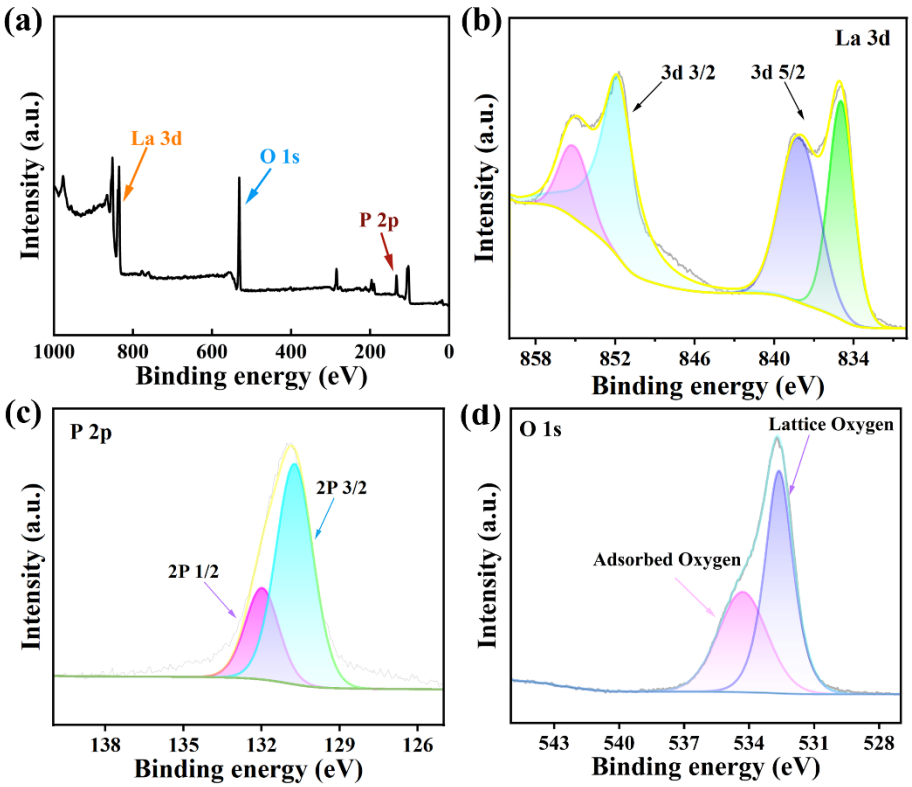

Fig. S1. The XPS spectra of $LaPO_4$. (a) Survey spectrum, (b-d) high-resolution XPS spectra of La 3d, P 2p and O 1s.

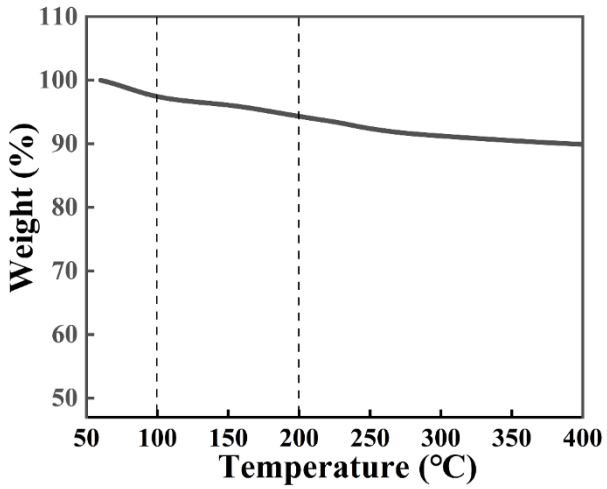

Fig. S2. The thermogravimetric (TG) curve of $LaPO_4$.

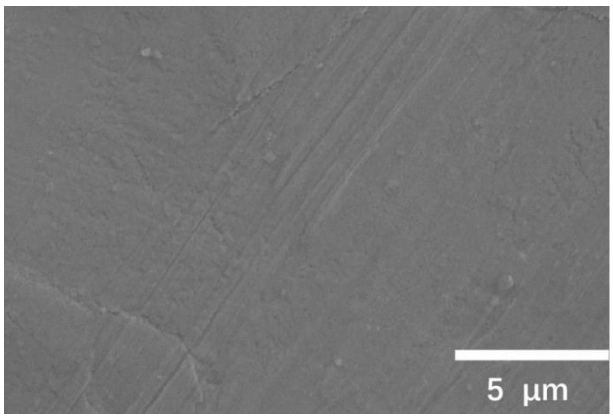

Fig. S3. The optical photograph of pure Zn sheet.

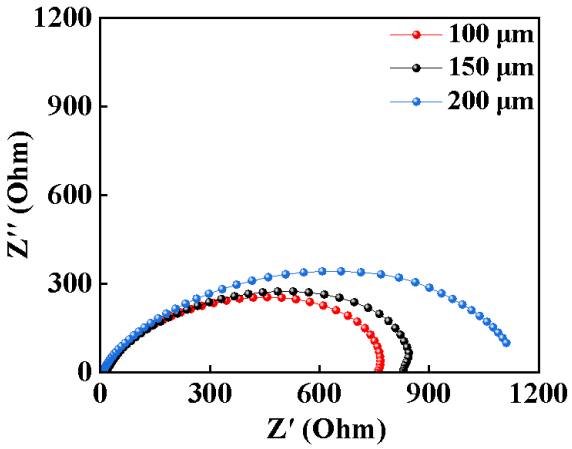

Fig. S4. EIS curves of LAP-Zn symmetrical cells with various thicknesses.

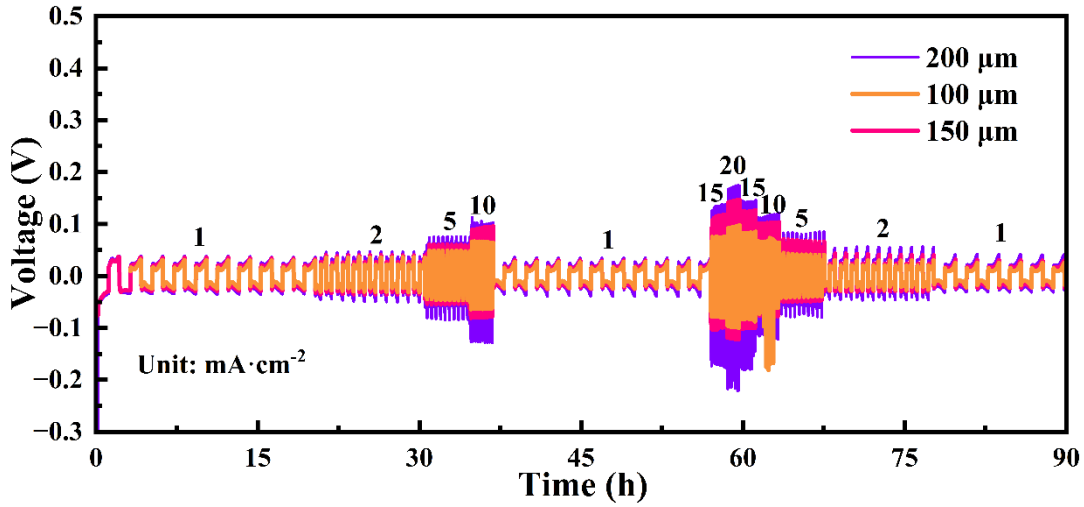

Fig. S5. Rate performance of LAP-Zn symmetrical cells with various thicknesses with a capacity of 1 mAh cm^{-2}.

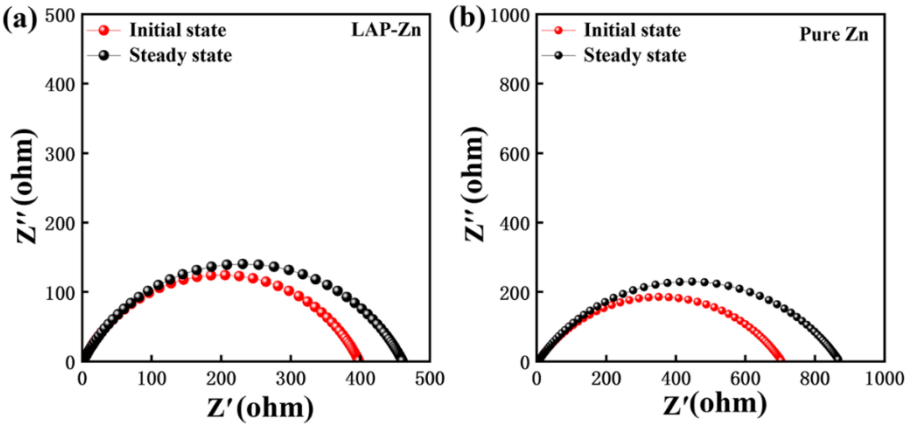

Fig. S6. The EIS curves of pure Zn and LAP-Zn before and after polarization process under a voltage of 10 mV for 400 s.

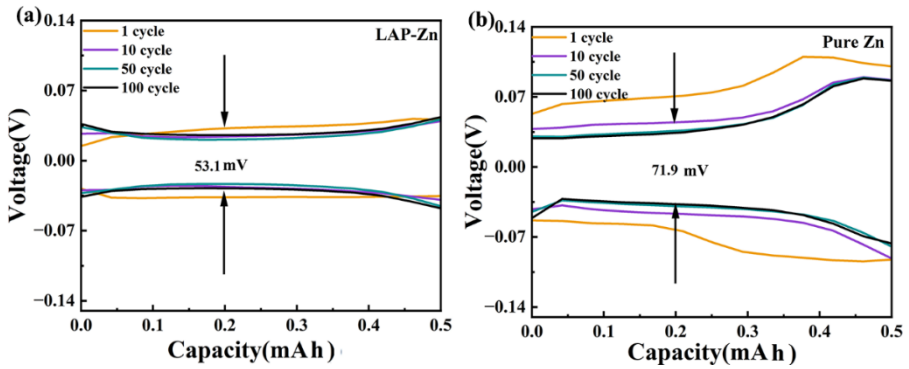

Fig. S7. The Zn plating/stripping curves of symmetric cells at 5 mA cm^{-2}, 1 mAh cm^{-2}.

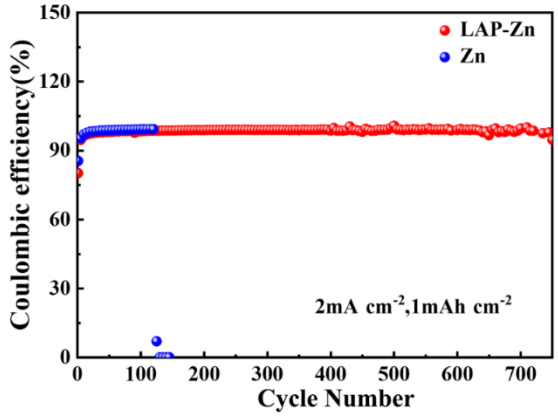

Fig. S8. CEs of asymmetric Zn//Cu cells at 2 mA cm^{-2}, 1 mAh cm^{-2}

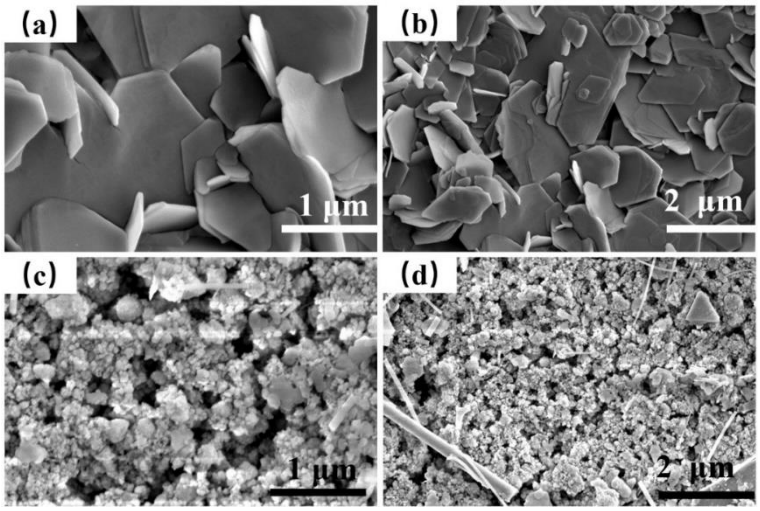

Fig. S9. SEM images of the Zn anode cycled in Zn//Cu half-cell: (a-b) pure Zn, (c-d) LAP-Zn.

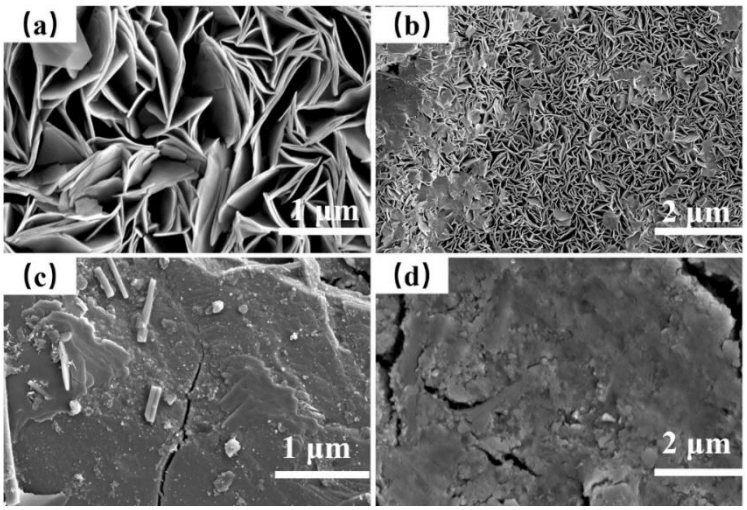

Fig. S10. SEM image of Zn anode cycled in Zn//AC zinc ion capacitor: (a-b) pure Zn, (c-d) LAP-Zn.

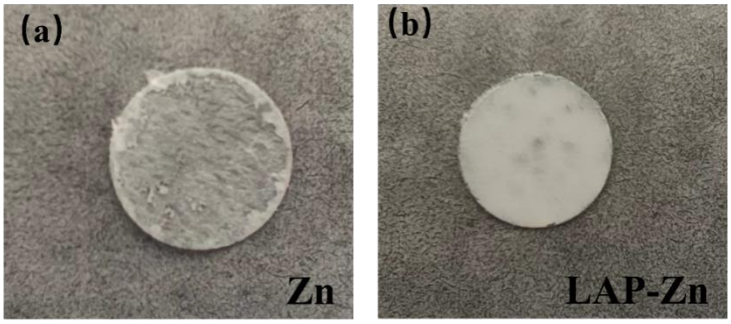

Fig. S11. The digital photos of LAP-Zn and Zn in symmetrical cells after 100 cycles at 2 mA cm^{-2}, 1 mAh cm^{-2}

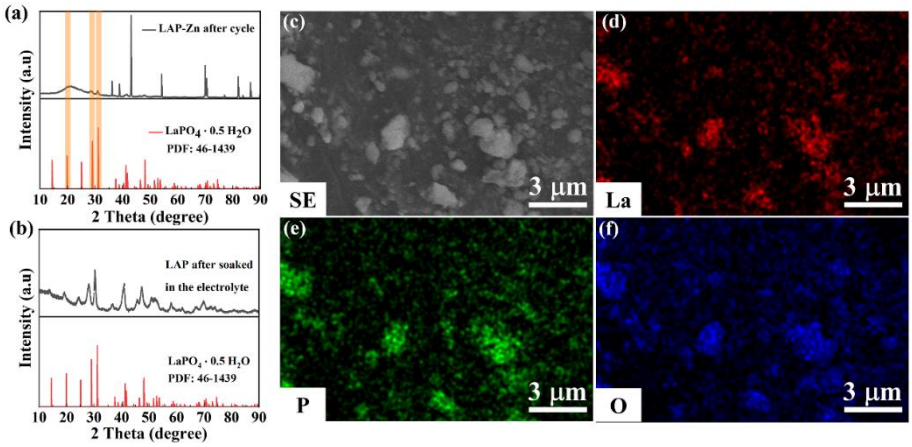

Fig. S12. (a) XRD spectrum of LAP-Zn anode after 100 cycles at 2 mA cm^{-2}, 1 mAh cm^{-2}. XRD spectrum (b), SEM image and EDS mapping results (c-f) of LAP powder after soaked in the electrolyte for 7 days.

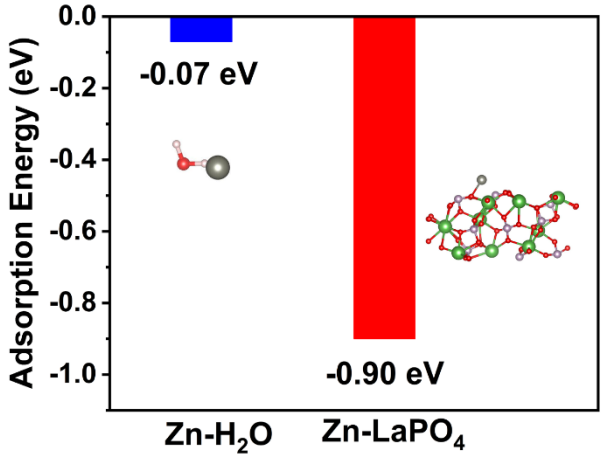

Fig. S13. The calculated adsorption energy of Zn with H_2O and LAP.

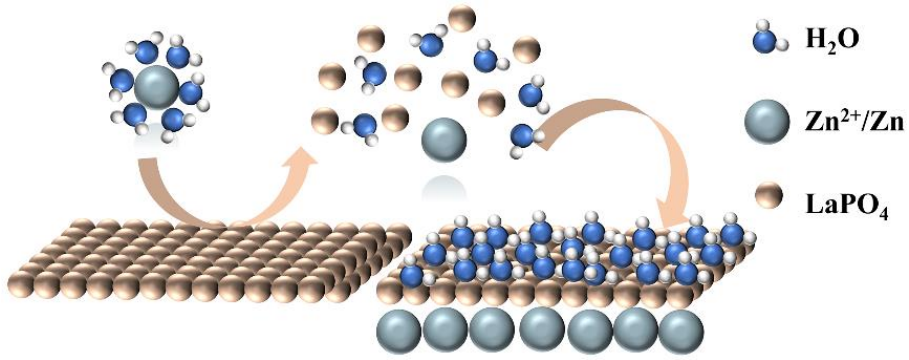

Fig. S14. Performance improvement mechanism diagram for "hydrophilic-Zn^{2+} conductive" LAP layer

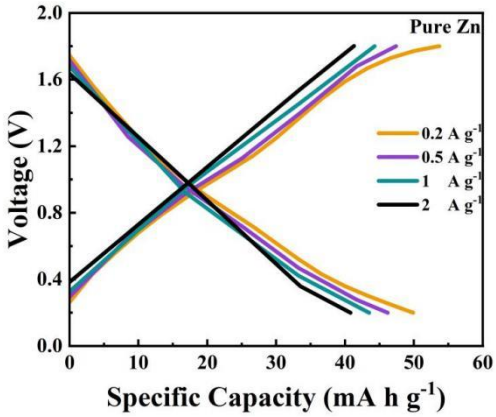

Fig. S15. The charge/discharge curves of pure Zn//AC zinc ion capacitor at various current densities.

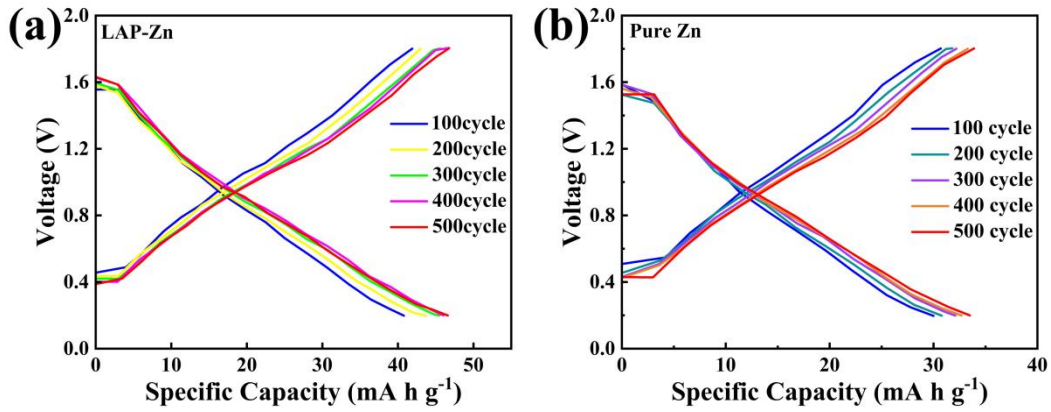

Fig. S16. The charge/discharge curves of pure Zn//AC and LAP-Zn//AC cells at different cycle.

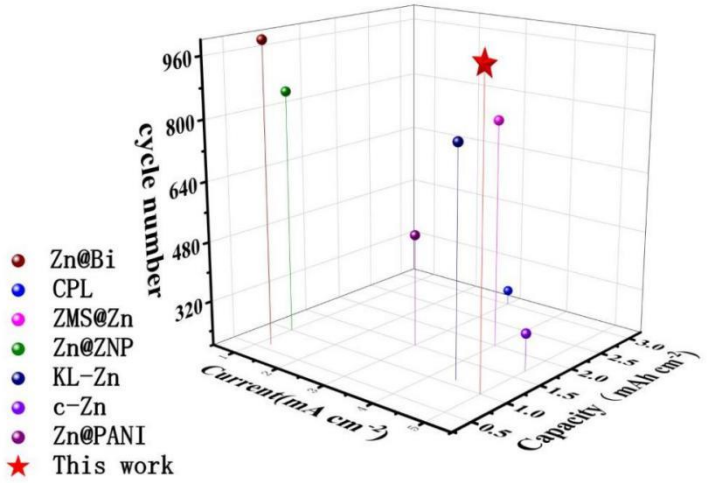

Fig. S17. Comparison of the performance of LAP-Zn with previously reported Zn anodes.

Table S1. The comparison between this work and previously reported works

Zn anode	Current density and capacity	Lifespan	Reference
LAP-Zn	5 mA cm^{-2}, 1 mAh cm^{-2}	1000 h	This work
Zn@Bi	1.2 mA cm^{-2}, 0.6 mAh cm^{-2}	1000 h	[4]
CPL	3 mA cm^{-2}, 3 mAh cm^{-2}	240 h	[5]
ZMS@Zn	4 mA cm^{-2}, 2 mAh cm^{-2}	800 h	[6]
Zn@ZNP	1 mA cm^{-2}, 1 mAh cm^{-2}	850 h	[7]
KL-Zn	4.4 mA cm^{-2}, 1.1 mAh cm^{-2}	800 h	[8]
c-Zn	5 mA cm^{-2}, 1.68 mAh cm^{-2}	300 h	[9]
Zn@PANI	3 mA cm^{-2}, 1.5 mAh cm^{-2}	500 h	[10]

References

[1] G. Kresse; J.Furthmüller; Efficiency of ab-initio total energy calculations for metals and semiconductors using a plane-wave basis set, *Comput. Mater. Sci.*, 1996, 6 (1), 15-50.

[2] P. E. Blochl; Projector augmented-wave method, Phys. Rev. B Condens. *Matter*, 1994, 50 (24), 17953-17979.

[3] J. P. Perdew; J. A. Chevary; S. H. Vosko; K. A. Jackson; M. R. Pederson; D. J. Singh; Fiolhais, C., Atoms, molecules, solids, and surfaces: Applications of the generalized gradient approximation for exchange and correlation. Phys. Rev. B Condens. *Matter*, 1992, 46 (11), 6671-6687.

[4] Y Du; Y Feng; R Li; Z Peng; X Yao; S Duan, Zinc-Bismuth Binary Alloy Enabling High-Performance Aqueous Zinc Ion Batteries, *Small*, 2024, 20(17): 2307848.

[5] J Yin; M Li; X Feng; T Cui; W Sun; M Wang, Comprehensive protection of Zn metal anode via caprolactam towards highly stable aqueous zinc ions batteries, *J. Alloys Compd.*, 2024, **971**: 172785.

[6] L Pan; H He; Q Yan; P Hu; Ultra-strong zinc-ion adsorption layer constructed by zeolite molecular sieve for advanced aqueous zinc-ion batteries, *J. Power Sources*, 2023, **571**: 233090.

[7] Y Chen; W Wang; W Zhao; J Xu; P Shi; Y Min; Nano-semiconductor material stabilized Zn metal anode for long-life aqueous Zn-ion batteries, *J. Colloid Interface Sci.*, 2023, **650**: 593.

[8] C Deng; X Xie; J Han; Y Tang; J Gao; C Liu;, A Sieve-Functional and Uniform-Porous Kaolin Layer toward Stable Zinc Metal Anode, *Adv. Funct. Mater.*, 2020, **30**(21): 2000599.

[9] B Sui; L Sha; P Wang; Z Gong; Y Zhang; Y Wu,, In situ zinc citrate on the surface of Zn anode improves the performance of aqueous zinc-ion batteries, *J. Energy Storage*, 2024, **82**: 110550.

[10] B Li; S Liu; Y Geng; C Mao; L Dai; L Wang, Achieving Stable Zinc Metal Anode Via Polyaniline Interface Regulation of Zn Ion Flux and Desolvation, *Adv. Funct. Mater.*, 2024, 34(5): 2214033.